STI and DTI: Tensor Characteristics and a Machine-Learning Approach to Estimate Susceptibility Tensors

Dimitrios Gkotsoulias[1], Riccardo Metere[2], Yanzhu Su[1], Cornelius Eichner[1], Torsten Schlumm[1], Alfred Anwander[1], Carsten Jäger[1], André Pampel[1], Catherine Crockford[3], Roman Wittig[3], Chunlei Liu[4], Harald E. Möller[1]

[1]Max Planck Institute for Human Cognitive and Brain Sciences, Leipzig, Germany, [2]Donders Institute for Brain, Cognition and Behaviour, Nijmegen, The Netherlands, [3]Max Planck Institute for Evolutionary Anthropology, Leipzig. Germany, [4]EECS, UC Berkeley, California, USA

gkotsoulias@cbs.mpg.de

MAX PLANCK INSTITUTE
FOR HUMAN COGNITIVE AND BRAIN SCIENCES

Introduction

There is increasing interest in linking brain pathologies to local alterations of iron or myelin content, and, hence, their precise quantitative assessment, for example by quantitative susceptibility mapping (QSM) [1,2].

Susceptibility has been shown to be anisotropic, especially in white matter (WM) regions, due to the specific arrangement of lipids enevloping myelinated fibers [3]. In susceptibility tensor imaging (STI) [4], susceptibility is depicted as a 2nd rank symmetric tensor, in a similar way as in diffusion tensor imaging (DTI) [5]. However, the quality *in vivo* STI is limited due to the need for multiple re-orientations of the object inside the main magnetic field [6].

Here, we use *post mortem* chimpanzee data to:

- Establish and validate a robust QSM/STI processing pipeline [7,8].
- Analyze and compare STI- and DTI-based tensor metrics in WM [4].
- Compare WM susceptibility estimates derived with the QSM pipeline from individual orientations with a reference susceptibility map calculated using STI [9].
- Develop a deep learning procedure to predict susceptibility tensors from DTI data and QSM results from a single orientation. This is motivated by the fact that, despite different physical origins underlying STI and DTI contrast, their orientation dependence is primarily defined by the presence of fiber bundles.

Methods

Data acquisitions for STI and DTI

Formalin-fixed brain from juvenile chimpanzee (Taï National Forest, Ivory Coast) that had died from natural causes.

- **STI**: MAGNETOM 7T, 32ch coil, ME-FLASH, TE: (4, 15)ms, 0.8mm isotr., matrix: $192 \times 192 \times 192$, 60 orientations.
- **DTI**: MAGNETOM Skyra Connectom, 32ch coil, dw segm. ME-EPI, TR: 6105ms, TE: (45, 50.9, 56.8, 62.7, 68.6)ms, 0.8mm isotr., matrix: $120 \times 160 \times 80$, 60 gradient directions.

QSM/STI pipeline steps

- **Phase unwrapping (#1)**: Laplacian-based method [10], STI Suite 3.0 [4].
- **Background-field removal (#3)**: V-SHARP method, STI Suite 3.0 [4].
- **Field to source inversion (#5)**: iLSQR method, STI Suite 3.0 [4].

Additional steps, results poccesing and tensor analysis:

- **Registrations (**STI orientations to reference and STI to DTI): FSL FLIRT–FMRIB's Registration Toolbox V.6 [11], Elastix Toolbox [12].
- **STI tensor analysis:** Python, MATLAB scripting.
- **DTI tensor analysis:** FSL-FMRIB Diffusion Toolbox 3.0 (FDT) [11].

Statistical analysis and machine learning:

- **Stats**: MATLAB stats toolbox, image processing toolbox.
- **Machine learning (ML):** Keras (Python), 3-layer sequential network, nonlinear activation functions, data pre-processing.

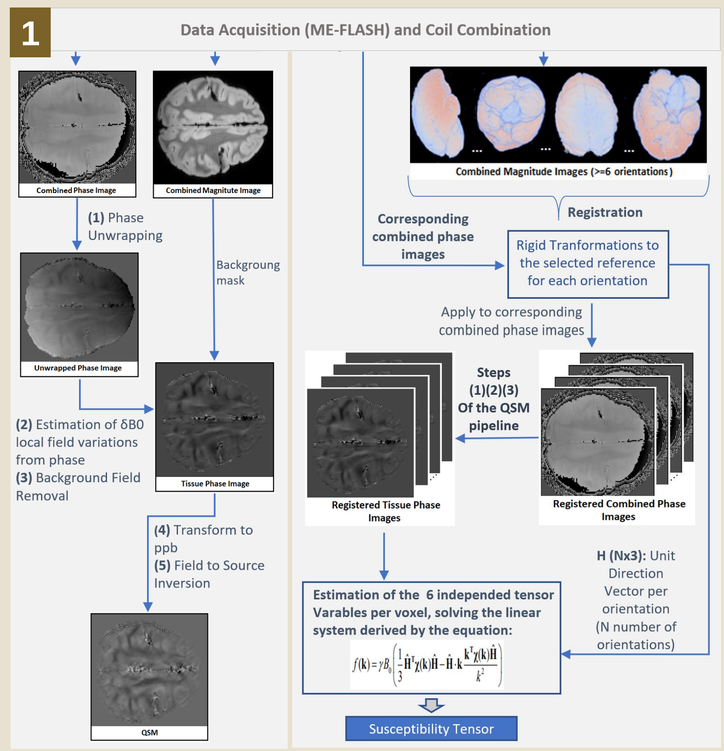

Figure 1. QSM and STI pipelines.

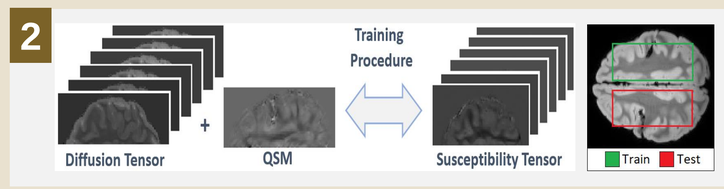

Figure 2. Machine learning process.

Results

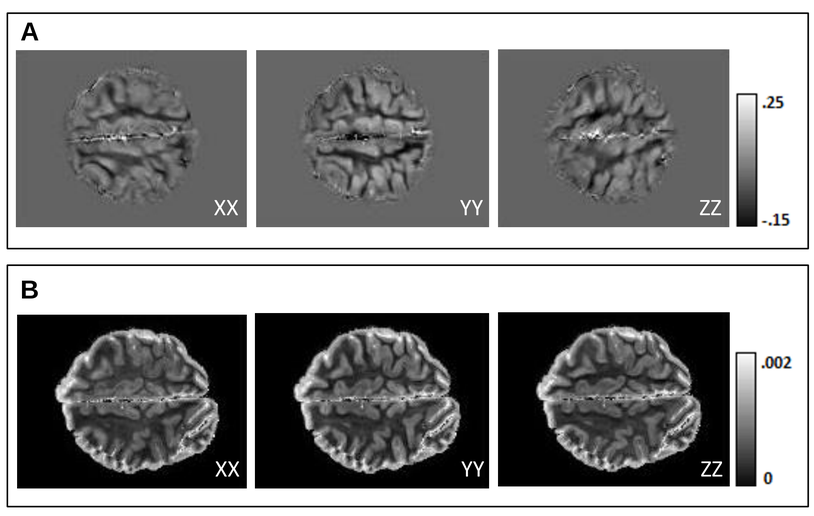

Figure 3. The three main tensor components (diagonal) from STI **(A)** and DTI **(B)**. The differentiation of WM is achieved, with lower values as compared to gray matter (GM) in DTI and mostly negative values in STI. Results are consisted with current bibliography [2,4]. Note that the susceptibility tensor has been reversed for further analysis [4].

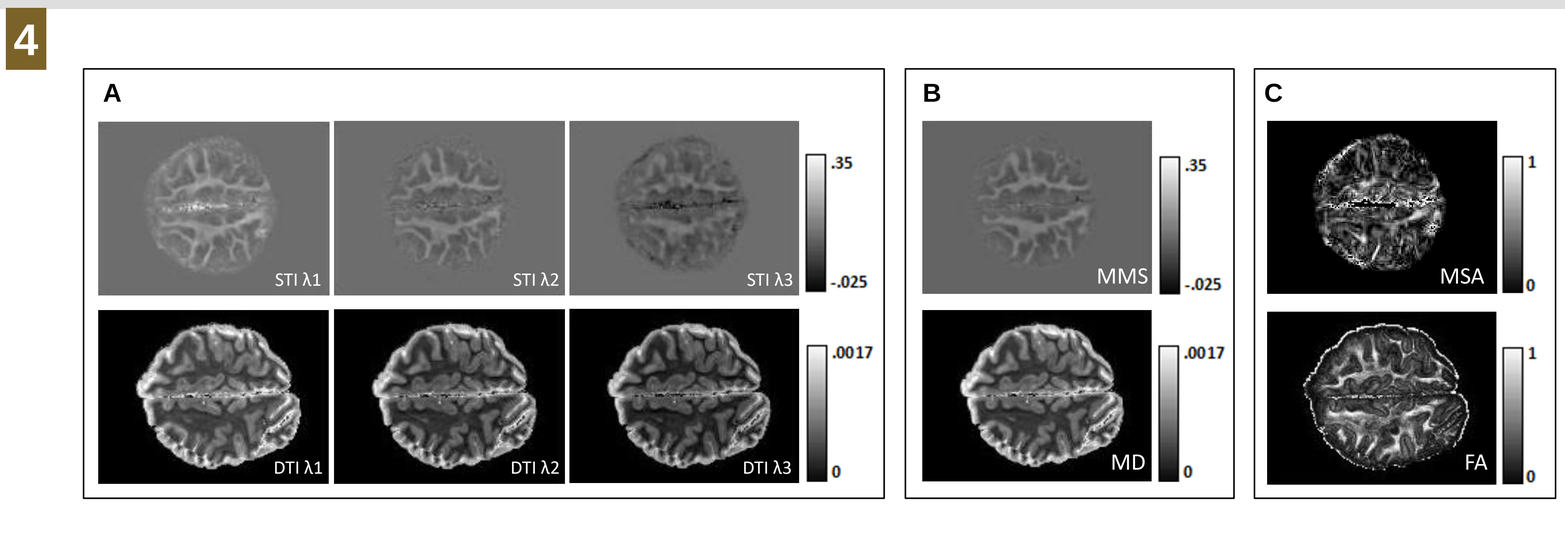

Figure 4. **(A)** Eigen-decomposition analysis and metrics derivation from the two tensors. Eigenvalues from both tensors follow the same trend of λ1>λ2≈λ3. **(B)** Maps of mean diffusivity (MD) and mean magnetic susceptibility (MMS) show the means of the eigenvalues for each method. Note the differentiation between GM and WM in both metrics. **(C)** Fractional anisotropy (FA) and magnetic susceptibility anisotropy (MSA) indicate the amount of anisotropy per voxel for the corresponding method (both running from 0 to 1).

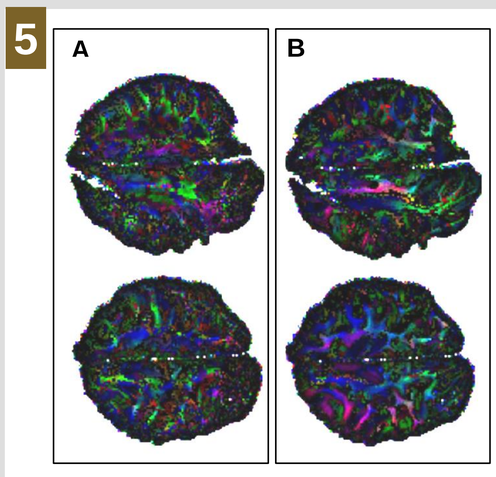

Figure 5. Two examples of corresponding slices of the principal eigenvector of STI **(A)** and DTI **(B)**, color-coded and weighted by the diffusion FA [4].

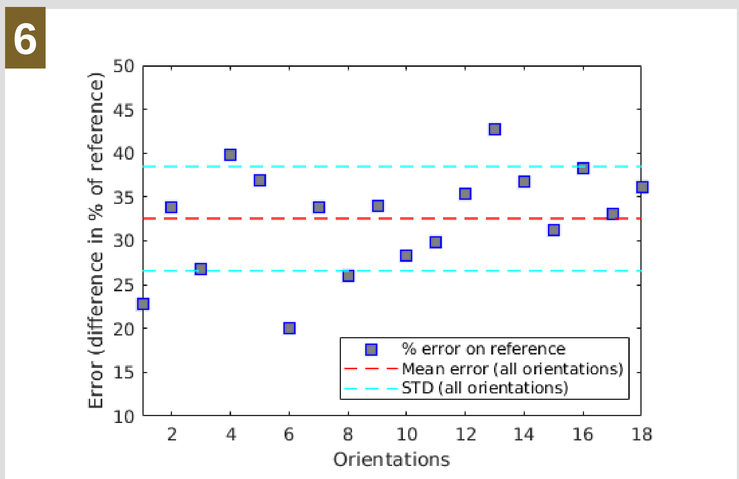

Figure 6. Mean error of the values of susceptibility calculated by STI (MMS) and by our QSM pipeline in each orientation in three selected WM areas. The error (absolute difference) is expressed as percent of the reference.

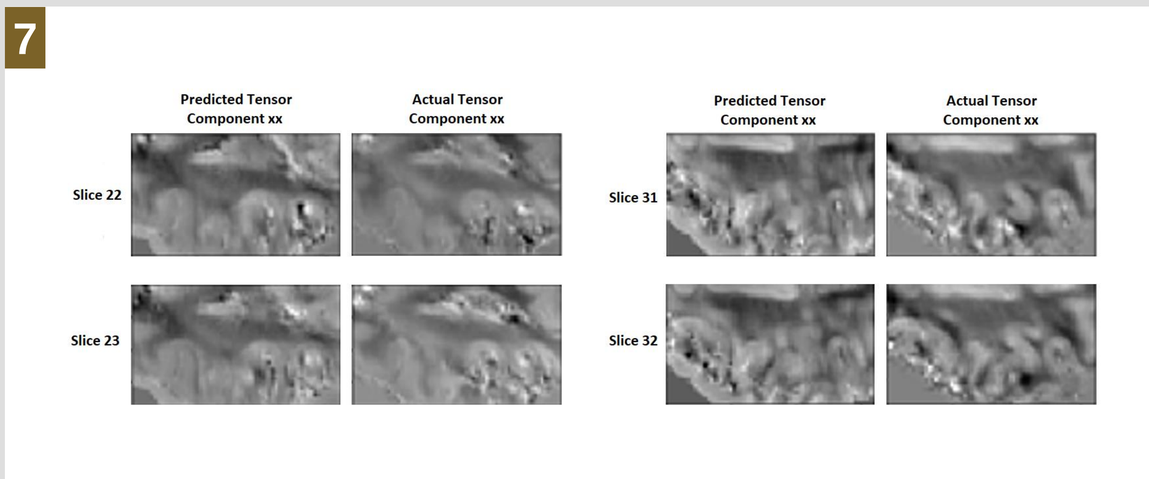

Figure 7. Four slices of preliminary results to predict susceptibility tensors from diffusion tensors and QSM data recorded from a single orientation using Deep Sequential Network in Keras (Python).

Discussion

Result highlights:

- ❑ In the first part of the project, the QSM and STI pipelines seem to have robust results. The two tensors appear to differentiate very well between WM and GM, while further analysis shows resemblence in anisotropy and primary eigenvectors.
- ❑ On the ML part, the predictions show promising correspondence, however, at currently still limited accuracy. The susceptibility tensor shows more variability in WM compared to the diffusion tensor and suffers from acquisition and post-processing artifacts. The final results are also impacted by residual registration limitations between STI and DTI.

Future work:

- ❑ Further improvement of registration as well as QSM/STI pipeline.
- ❑ Acquisition of more high-resolution DTI and STI data.
- ❑ More advanced descriptions of fiber orientation distributions (e.g., Bingham metrics [13]).
- ❑ Improvements of the ML part through:
  - STI artifact reduction.
  - improved WM isolation (specific fiber bundles).
  - Improved registration of STI and DTI.
  - Larger data base.
  - Better network selection and parameterization.

References

[1]: H.E. Möller et al., *Trends Neurosci.* (2019).
[2]: A. Deistung et al., *NMR Biomed.* (2017).
[3] S. Wharton & R. Bowtell, *Proc. Natl. Acad. Sci. USA* (2012).
[4] W. Li et al., *NeuroImage* (2012).
[5]: S. Mori & J. Zhang, *Neuron* (2006).
[6]: B. Bilgic et al., *NeuroImage* (2016).
[7]: C. Liu et al., *J. Magn. Reson. Imaging* (2015)
[8]: C. Liu, *Magn. Reson. Med.* (2010).
[9]: C. Langkammer et. al., *Magn. Reson. Med.* (2018).
[10]: M.A. Schofield & Y. Zhu, *Opt. Lett.* (2013).
[11]: M. Jenkinson et al., *NeuroImage* (2012).
[12]: S. Klein et al., *IEEE Trans. Med. Imaging* (2010).
[13]: T.W. Riffert et al., *NeuroImage* (2014).